Influence of the Fluorination of Iron Phthalocyanine on the Electronic Structure of the Central Metal Atom

Katharina Greulich, Martin Trautmann, Axel Belser, Sven Bölke, Reimer Karstens, Peter Nagel, Stefan Schuppler, Michael Merz, Angelika Chassé, Thomas Chassé, and Heiko Peisert*

ABSTRACT: The electronic structure of the central Fe ion of iron phthalocyanine (FePc) and perfluorinated iron phthalocyanine ($FePcF_{16}$) in thin films is investigated by X ray absorption spectroscopy (XAS) and X ray magnetic circular dichroism (XMCD), supported by photoemission. Both molecules grow in a flat lying adsorption geometry in thin films. Fe L edge X ray absorption spectra of FePc and $FePcF_{16}$ exhibit minor, but distinct, differences of the shape, indicating a different electronic structure. A significantly stronger XMCD signal and thus larger magnetic moments were observed for FePc compared to $FePcF_{16}$ at low temperatures (15 K). Multiplet calculations have been used to simulate the XA and XMCD spectra and give detailed insight into the electronic structure of Fe in FePc and $FePcF_{16}$. We suppose that the electronic structure crucially depends on the detailed arrangement of FePc and $FePcF_{16}$ molecules in thin films.

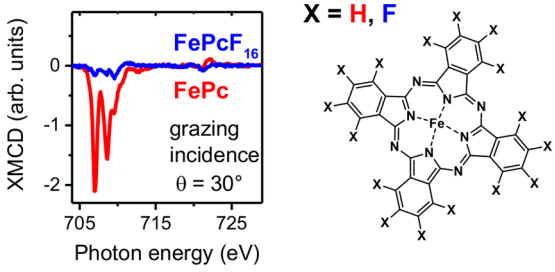

1. INTRODUCTION

Because of their unique optical, electronic, and magnetic properties, transition metal phthalocyanines (TMPcs) have been extensively investigated.[1,2] A broad variety of applications of metal phthalocyanines are known, among them optoelectronic devices,[3−9] in which the electronic structure in thin films is of particular importance. Most recently, magnetic properties came in the focus of interest for future applications in quantum information processing[10] and organic spintronics.[11−15]

At interfaces, the electronic configuration of the central metal atom of the TMPc and thus the magnetic properties might be distinctly affected by substrate properties.[12,16−21] Different ground states were reported for monolayer or few layer FePc on different substrates, for example, a mixed $^3B_{2g}$−^3E_g on Au(111),[22] $^3B_{2g}$ on Ag(001),[23] and a $^3A_{2g}$ on Si.[24] Magnetic properties of transition metal phthalocyanines on metal surfaces can be modified by magnetic coupling to the substrate,[20] which can suppress their local magnetic moment.[12,18] A graphene buffer layer between a ferromagnetic substrate and the phthalocyanine layer can be inserted to modify the magnetic interaction[25,26] or tune the charge transfer at the interface.[27] In this context, graphene may even enable a ferromagnetic or antiferromagnetic coupling.[25,26] The coupling between central metal ion and a magnetic layer is often mediated by the organic ligands.[20,28−30] Another route to tune electronic properties at interfaces might be a chemical doping.[23,31] For FePc monolayers on Cu(100), three different spin configurations of the Fe ion have been observed upon exposure to NO_2.[32]

In general, magnetic properties of transition metal compounds depend strongly on the transfer of charge between d orbitals and delocalized ligand states.[22,33] In particular, iron complexes are very flexible in their spin state,[34,35] and the electronic ground state of Fe in FePc has not yet been completely understood.[11−15,22,23,25,31,33,36−42] It was reported that FePc is paramagnetic at room temperature and can become ferromagnetic as a function of the relative Fe−Fe distance at low temperature.[43] In bulk α FePc, ferromagnetism was observed below 10 K.[44] However, a large variety of ground state configurations for FePc in thin films or single crystals have been proposed, including ^3E_g,$^3B_{2g}$, and $^3A_{2g}$.[45] This is caused by the fact that d_{z^2} (a_{1g}), d_{xy} (b_{2g}), and d_{xz}/d_{yz} (e_g) orbitals are energetically close to each other. Only $d_{x^2-y^2}$ (b_{1g}) orbitals are located at a significantly higher energy, and therefore they are unoccupied.[46] Most studies agree that for films with a columnar stacking (α FePc) the configuration ^3E_g is expected to be associated with large orbital magnetic moments.[47,48] Two different ^3E_g ground state configurations are possible; both configurations were proposed for FePc: $(b_{2g})^2(e_g)^3(a_{1g})^1$[46,47,49] and $(b_{2g})^1(e_g)^3(a_{1g})^2$.[22,45,50] Recent publications stated that $^3B_{2g}$ multiplets for α FePc have no

influence on the ground state,[51,52] while others expect a significant contribution.[50]

A reason for the different results might be the crucial role of the detailed arrangement of the molecules. It was reported that the ground state of isolated FePc molecules is $^3A_{2g}$, and solely the stacking of the molecules in films or single crystals causes a change to a ^3E_g configuration.[47,48] In this study we focus on the electronic and magnetic structure of the Fe atom in FePc and $FePcF_{16}$ thin films. The fluorination of phthalocyanines may have a significant impact on the single crystal structure and arrangement in thin films.[53−56] As substrate we chose GeS(100) to avoid both magnetic coupling between substrate and molecule and chemical interactions as observed at more reactive metal substrates.[19,57]

Insight into the 3d electron states, as the origin of magnetic properties of the TMPcs, can be acquired by X ray absorption spectroscopy (XAS) and (soft) X ray magnetic circular dichroism (XMCD). XMCD is a technique that combines the local selectivity of X ray absorption spectroscopy with magnetic measurements. Monitoring the difference in absorption between right and left circularly polarized X rays (i.e., the incident circularly polarized X rays are either parallel (μ+) or antiparallel (μ) to the sample magnetization direction), XMCD gives information about the spin and angular momentum of the excited atom.[58,59] Alternatively, the X ray helicity can be kept constant, and the magnetization direction is switched.[60] The technique allows even the high sensitive detection of a weak induced magnetism in non magnetic elements, such as carbon at the graphene/Ni(111) interface.[61]

2. EXPERIMENTAL SECTION

The GeS(001) crystal was purchased from MaTeck GmbH. A pristine surface was prepared by cleaving in a vacuum with adhesive tape. The cleanliness was checked by XPS and low energy electron diffraction (LEED). FePc was purchased from Sigma Aldrich GmbH and $FePcF_{16}$ from Synthon Chemicals & Co KG. Both substances were resublimed for further purification. For *in situ* deposition onto the GeS substrate, home built Knudsen cells were used. The deposition temperature was 660 K, and the deposition rates (0.2−0.3 nm/min) were monitored by a quartz microbalance. Nominal layer thicknesses were estimated from XPS intensity ratios of overlayer and substrate core level peaks assuming layer by layer growth. For this, the sensitivity factors from Yeh and Lindau were used,[62] and the mean free paths were calculated according to Seah and Dench.[63]

X ray photoelectron spectroscopy (XPS), X ray absorption, and X ray magnetic circular dichroism measurements were performed at the WERA beamline of the Institute for Quantum Materials and Technologies (at the Karlsruhe Research Accelerator, Karlsruhe, Germany) equipped with the fast switching 7 T XMCD system from MPI IS Stuttgart. The base pressure in the multichamber UHV system was $<3 \times 10^{-10}$ mbar. XP spectra were recorded at an excitation energy of 890 eV; the energy resolution was set to 650 meV. For the N K and Fe $L_{2,3}$ X ray absorption (XA) spectra, the energy resolution was set to 220 and 340 meV at photon energies of 400 and 710 eV, respectively. The XA spectra were recorded in total electron yield (TEY) mode. The energy was calibrated to reproduce the energy of the Ni L_3 absorption edge of NiO at 853.0 eV. The photon flux I_0 of the incident synchrotron light monitored by a gold mesh was used for normalization. All spectra were normalized to equal step height well above the ionization threshold. Polarization dependent X ray absorption spectra were measured at different angles of the incident synchrotron light with respect to the sample surface (θ). "Normal incidence" corresponds to $\theta = 90°$ for all chosen polarizations, and "grazing incidence" corresponds to $\theta = 20°$ and $\theta = 30°$ for the experiments with p polarized (electric field polarized parallel to the plane of incidence) and circularly polarized light, respectively.

XMCD signals were obtained taking XA spectra with circularly polarized light in continuous mode; that is, for each spectrum either the helicity of the incident light was changed or, alternatively, the direction of the constant magnetic field of 7 T (parallel or antiparallel to the projection of the photon spin $\vec{k}$). Several data sets were averaged for μ_+ spectra (projection of the photon spin $\vec{k}$ parallel to sample magnetization direction) and μ_- spectra (projection of the photon spin $\vec{k}$ antiparallel to sample magnetization direction). To further remove measurement artifacts, we alternately changed the polarization of the synchrotron light and the direction of the sample magnetization to obtain μ_+ or μ_-. The XMCD signal was defined as the difference of μ_+ and μ_- spectra. The sample temperature was varied between room temperature and 15 K. The calculations have been performed by using the programs CTM4XAS,[64] CTM4DOC,[65] and Crispy.[66]

3. RESULTS AND DISCUSSION

3.1. Molecular Orientation and Electronic Structure in Thin Films. For an investigation of the electronic structure of molecules in thin films, information about the molecular orientation and stacking is crucial. For TMPcs, the knowledge of molecular orientation supports the assignment of angle dependent resonances in $L_{2,3}$ edge XA spectra of the central metal atom. Especially for iron phthalocyanines the electronic structure of the Fe ion may further depend on subtle differences of its surroundings, i.e., the detailed arrangement of neighboring molecules.[57,67]

The orientation of planar molecules can be probed by XAS (or near edge X ray absorption fine structure, NEXAFS) using linearly polarized synchrotron light.[68−70] Both C 1s π^* and N 1s π^* excitations can be used for determining the orientation of phthalocyanines. According to the orbital vector approach, maximal intensity of N 1s π^* transitions is observed if the electric field vector **E** of the incident synchrotron light is parallel to the p_z orbitals, i.e., normal to the molecular plane; vice versa, the intensity of transitions to orbitals with σ^* character will be maximal when **E** is parallel to the molecular plane.

The upper panel of Figure 1 shows the N K X ray absorption spectra of 3 nm thick FePc (Figure 1a) and perfluorinated $FePcF_{16}$ films on GeS at grazing incidence ($\theta = 20°$) and normal incidence ($\theta = 90°$). As depicted in the inset of Figure 1 illustrating the measurement geometry, θ is the angle between the incoming p polarized synchrotron light and the sample surface. The shape of N K edge XA spectra is very similar for thin films of FePc and $FePcF_{16}$. The general shape is common for phthalocyanines, where intensity at photon energies lower than 402 eV are essentially assigned to transitions into orbitals of π^* character, although weak σ^* transitions may also appear in the π^* region.[71] Despite their overall similarity, small differences between the FePc and $FePcF_{16}$ spectra are noticeable. As marked in Figure 1 (blue

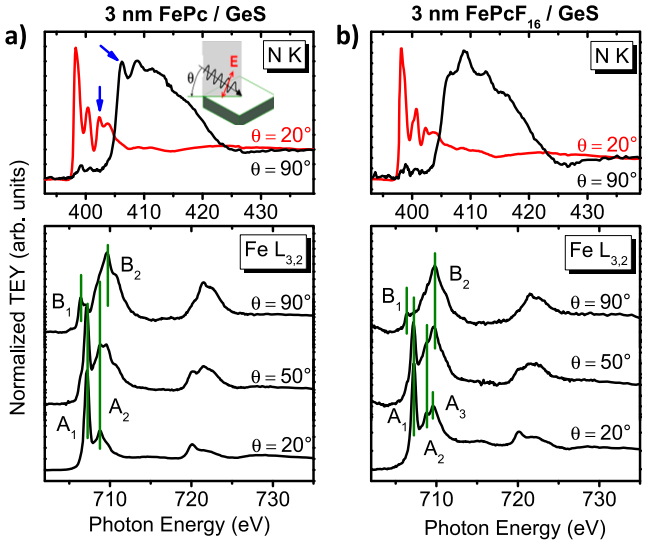

Figure 1. N K edge (top) and Fe $L_{2,3}$ edge (bottom) XA spectra of $FePcF_x$ films on GeS: (a) FePc (thickness 3.0 nm) and (b) $FePcF_{16}$ (thickness 3.0 nm). The very strong anisotropy in the N K edge spectra indicate almost flat lying molecules in both cases, in good agreement with related anisotropies observed in the Fe $L_{2,3}$ edge spectra. The overall shape of the Fe $L_{2,3}$ edges is also similar, but the line shape of $FePcF_{16}$ is slightly broader and the relative intensities of the peaks are different.

arrows), there are several features at photon energies of 402–408 eV at grazing incidence and at photon energies of 405–408 eV at normal incidence that look more distinct for FePc than for $FePcF_{16}$. For TMPcs, the electronic structure of the central metal atom may be significantly affected by hybridization between the d orbitals and the neighboring nitrogen π orbitals.[22,33] The different shape of the N K edge XA spectra points to a slightly different electronic structure at the nitrogen sites.

N K edge XA spectra for both FePc and $FePcF_{16}$ in Figure 1 show the same, very strong angular dependence. N 1s π^* transitions are most intense at grazing incidence, indicating a predominantly flat lying molecular orientation on the GeS substrate. Assuming uniform molecular tilt angles in the probed region and over the azimuthal angle, an averaged molecular tilt with respect to the substrate surface can be estimated from the intensity of π^* transitions at normal and grazing incidence according to[68]

$$I \sim P(\sin^2\alpha \sin^2\theta + 2\cos^2\alpha \cos^2\theta) + (1 - P)\sin^2\alpha \quad (1)$$

where P is the polarization degree, θ the angle of incidence of the p polarized synchrotron radiation, and α the tilt angle. With $P = 0.93$ we obtain average tilt angles of 25° and 24° for the 3 nm thick films of FePc and $FePcF_{16}$ on GeS, respectively. A pure out of plane character of the two analyzed features at 397.0 and 401.0 eV was assumed. However, the maximum of the remaining intensity in the π^* region at normal incidence is not observed at the same energy (399.2 eV) as the most intense π^* features at grazing incidence (398.3 eV), which may point to the presence of differently polarized transitions. Thus, our estimation might be understood as an upper limit for the molecular tilt. We note that these tilt angles are averaged over the whole sample, and thus different distributions of polar tilt angles might be present for both samples. In particular, the similar average orientation does not imply a similar arrangement of molecules in the film.

At first glance, also Fe $L_{2,3}$ edge spectra in the bottom panels of Figure 1 are similar for FePc and $FePcF_{16}$. The shape of the XA spectra is typical for iron phthalocyanines, in good agreement with the literature.[16,17] In addition, no significant differences were observed in the corresponding Fe $2p_{3/2}$ core level photoemission spectra for both molecules (cf. Figure S1 of the Supporting Information). Although the shape of the transition metal $L_{2,3}$ XA spectra is determined to a large extent by multiplet effects, caused by the strong overlap of the core wave function with the valence wave functions (see e.g. ref 72), the angular dependence of particular features can be generally attributed to transitions into different unoccupied d orbitals. For the almost flat lying FePc and $FePcF_{16}$ molecules, transitions into orbitals located in the molecular plane (e.g., states of $d_{x^2-y^2}$ and d_{xy} character) are intense at normal incidence, whereas transitions into orbitals with out of plane components will be probed mainly at grazing incidence by using linearly p polarized radiation (e.g., of states d_{xz}, d_{yz}, and d_{z^2} states character). Because of in plane components of the d_{xz}, d_{yz}, and d_{z^2} orbitals, they contribute also to spectral features at normal incidence.[50]

Because transition metal $L_{2,3}$ edge spectra are largely governed by multiplet effects, the features cannot be assigned to specific transitions without theoretical considerations. Nevertheless, we will briefly discuss the nature Fe L_3 transitions in Figure 1 based on their angular dependence. At grazing incidence, both FePc and $FePcF_{16}$ spectra exhibit a very intense peak denoted A_1 at 707.8 eV. At normal incidence in contrast, a low intensity feature denoted B_1 appears, followed by a broad feature denoted B_2 at about 709 eV. Considering that the molecules are flat lying on the surface, the A features will arise from out of plane transitions, while the B features are essentially from transitions within the molecular plane. Although both FePc and $FePcF_{16}$ spectra show the same sequence of peaks, differences in relative intensities can be detected. The most notable difference is the more prominent A_1 peak at grazing incidence for FePc compared to $FePcF_{16}$. At the high energy side of A_1, the lower intensity features (including A_2 and A_3) are more pronounced in the case of $FePcF_{16}$. The feature denoted A_3, which is dominant for $FePcF_{16}$, appears only as a small shoulder for FePc. We note that these features cannot be understood by the presence of in plane polarized B_2 features at grazing incidence (e.g., due to a tilt of the molecules). The green lines in Figure 1 make clear that the energetic position of A_1 and A_2 is different than B_2. Because both FePc and $FePcF_{16}$ are essentially flat lying on the substrate surface and molecular tilt angles are very similar for both molecules, we ascribe the differences in the shape of Fe $L_{2,3}$ edge spectra to subtle changes of the electronic structure of the Fe atom caused by the fluorination of the phthalocyanine. The complexity of A_1 and A_2 may indicate that they arise from a variety of different excitations. We note that apparent differences are basically the same for FePc and $FePcF_{16}$ films on van der Waals surfaces, e.g., MoS_2,[73] and can be even more pronounced for FePc and $FePcF_{16}$ on crystalline metal substrates.[57,67]

3.2. XMCD Spectra of FePc and $FePcF_{16}$. To study the electronic structure of the Fe ion in FePc and $FePcF_{16}$ more in detail, XMCD experiments were performed. We chose a temperature of 15 K, which is above the Curie temperature of

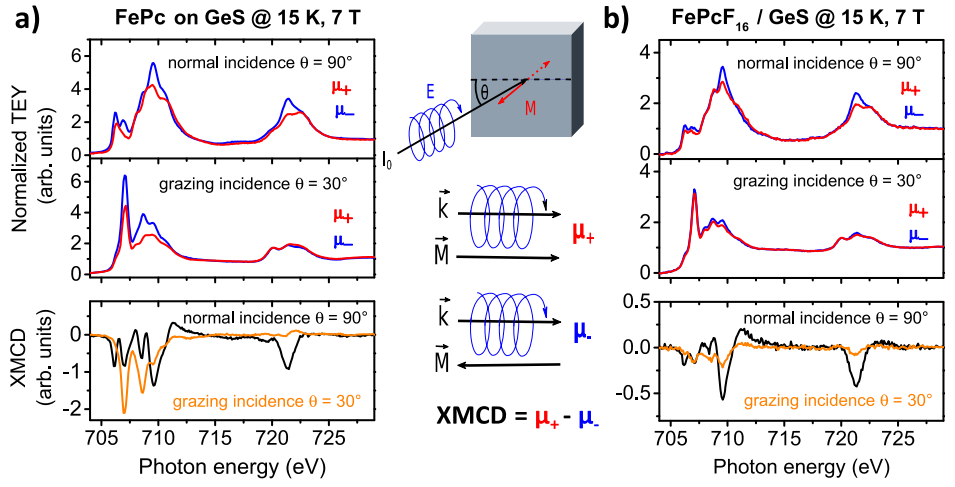

Figure 2. Absorption at the Fe $L_{2,3}$ edges of (a) 3 nm FePc and (b) 3 nm $FePcF_{16}$ on GeS, measured with the projection of the photon spin $\vec{k}$ either parallel (μ_+, red spectra) or antiparallel (μ_-, blue spectra) to the sample magnetization direction at normal and grazing incidence. The XMCD spectra calculated as $\mu_+ - \mu_-$ are shown in the lowest panel for both directions of incident light.

Table 1. Magnetic Moments m_l and m_s^{eff} as Determined from the XMCD Spectra (7 T, 15 K) of 3 nm FePc and $FePcF_{16}$ on GeS[a]

	$m_l/n_h/\mu_B$	$m_s^{eff}/n_h/\mu_B$	$m_l^{xy}/n_h/\mu_B$	$m_s/n_h/\mu_B$
FePc grazing incidence	0.17(±0.02)	0.22(±0.03)	0.19(±0.03)	0.19(±0.03)
FePc normal incidence	0.10(±0.004)	0.02(±0.01)		
$FePcF_{16}$ grazing incidence	0.02(±0.01)	0.03(±0.02)	0.02(±0.01)	0.02(±0.02)
$FePcF_{16}$ normal incidence	0.03(±0.005)	0.03(±0.008)		

[a]All values are normalized to the number of holes n_h.

bulk α FePc (10 K).[44] The Curie temperature of FePc thin films has been reported to be even lower.[74] First, a hysteresis curve was measured, as shown in Figure S2. The absence of an open loop indicates the presence of a paramagnetic phase. In Figures 2a and 2b, we show XMCD spectra of 3 nm FePc and $FePcF_{16}$ thin films on GeS acquired at normal and grazing incidence of the circularly polarized light at 15 K and 7 T. The spectra denoted μ_+ were measured with the k vector of the incident light parallel to the sample magnetization direction. While measuring the spectra denoted μ_-, the **k** vector of the incident light and the sample magnetization direction were oriented antiparallel. The XMCD spectra are calculated as $\mu_+ - \mu_-$ (Figure 2, lower panels).

A magnetic dichroism is clearly visible in the Fe $L_{3,2}$ edge spectra of both molecules, FePc and $FePcF_{16}$. The XMCD spectra for FePc, the magnetic *xy* anisotropy, and the resulting magnetic moments (Table 1) according to the XMCD sum rules are in good agreement with the literature, although FePc was grown on other substrates.[18,74,75]

The XMCD of the $FePcF_{16}$ thin film in Figure 2 differs distinctly from the XMCD of the FePc thin film. Although the features of the $FePcF_{16}$ XMCD spectrum at normal incidence appear also in the corresponding FePc spectrum, the intensity is reduced by a factor of about 2. At grazing incidence, the reduction of the magnetic dichroism of $FePcF_{16}$ is even more pronounced, and the XMCD spectral features appear greatly changed in comparison to FePc at this angle of incidence. The very prominent peak in the FePc XMCD spectrum at 707.3 eV is almost completely missing for $FePcF_{16}$. This affects distinctly the angular dependent orbital and effective spin moments m_l and m_s^{eff}, summarized in Table 1. For the estimation of m_l and m_s^{eff} from the XMCD spectra, the XMCD sum rules were applied (see the Supporting Information for a detailed explanation).[58,59,76−79] Note that the values given in Table 1 are normalized to the number of holes n_h in all cases. Both m_l and m_s^{eff} are distinctly larger for the FePc thin film than for the $FePcF_{16}$ film. This difference is much larger for the data determined at grazing incidence. Assuming flat lying, azimu thally disordered molecules of D_{4h} symmetry, the angular dependent orbital moment can be split into components parallel (m_l^{xy}) and normal (m_l^z) to the substrate plane, and the spin moment m_s can be extracted from m_s^{eff}. According to the sum rule analysis (shown in more detail in the Supporting Information), especially the orbital moment in the substrate plane and the spin moment are about 5−10 times higher for FePc than for $FePcF_{16}$.

3.3. Multiplet Calculations. Multiplet calculations have proven to be a powerful tool to calculate Fe $L_{2,3}$ edge absorption spectra of transition metal phthalocyanines. Magnetic properties have been investigated for a number of different systems. For FePc a large variation of optical parameters *Dq* (crystal field interaction), *Ds*, and *Dt* have been used in calculations depending on layer thickness, substrate, and preparation conditions.[22−24,51,67,80] However, it is challenging to find appropriate calculation parameters to properly describe the experimental results since different parameters depend on each other and single calculations can be very time consuming. For the systems of FePc and $FePcF_{16}$ on GeS(001) we used a different approach. To simplify the process, we have developed a method using two parameter plots and automated calculations. Thus, the parameter space can be scanned rapidly to distinguish promising parameter combinations.

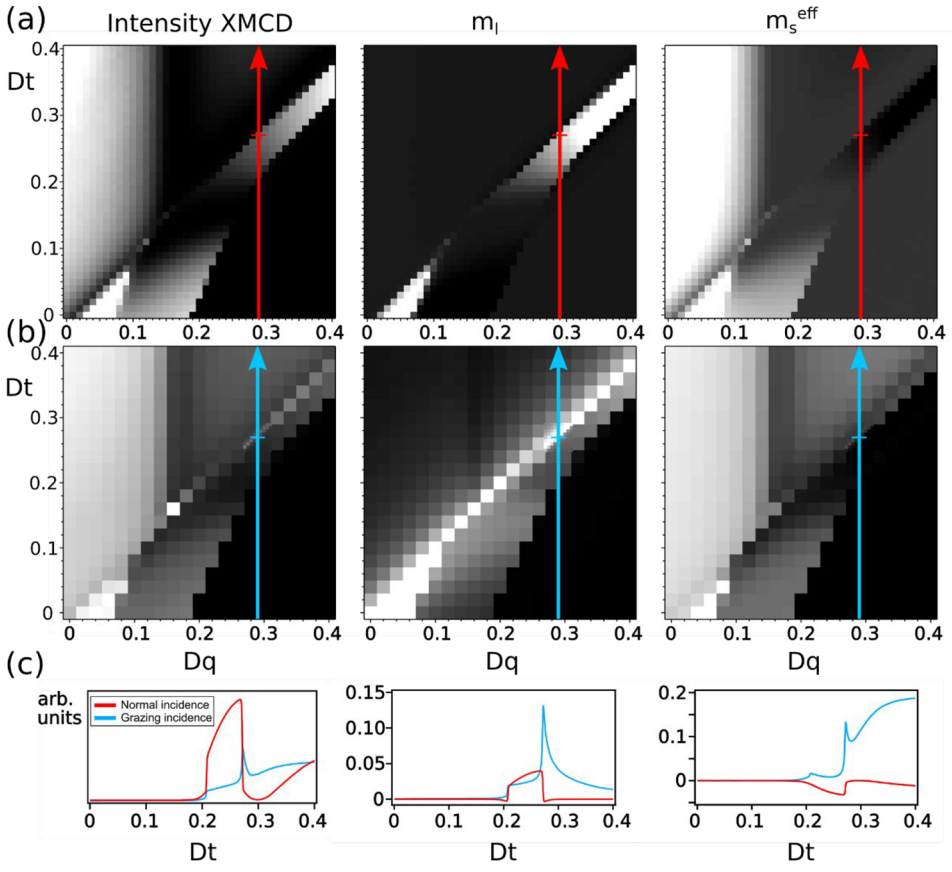

Figure 3. Two parameter plots of Fe^{2+} in FePc for (a) normal and (b) grazing incidence varying the calculation parameters *Dq* and *Dt* with fixed *Ds* = 0.50, SOC = 1.01, and Slater integrals reduced to 60%. In the grayscale black corresponds to low and white to high values for XMCD, m_l and m_s^{eff}, respectively. The line profiles in (c) are taken along the red and blue arrows. The crossings of the short colored horizontal bars with the vertical arrows mark the calculation parameter used for FePc.

XAS of the $L_{2,3}$ edges were calculated for a Fe^{2+} ground state (electron configuration $2p^63d^6$) with D_{4h} symmetry. This adopts the planar symmetry of FePc with four nitrogen atoms as next neighbors. The temperature of 15 K and the magnetic field of 7 T were fixed according to the experimental conditions Both programs calculate spectra on the basis of the optical parameters *Dq*, *Ds*, and *Dt* as well as Slater integrals (Coulomb interaction of d and p electrons) and spin−orbit coupling (SOC).[81] A ligand to metal charge transfer (LMCT) was also implied in the calculations. This adds a small portion of a Fe^+ ground state ($2p^6$ $3d^7$). The calculation parameters for the LMCT were estimated from multiplet structures of Fe 2p photoemission spectra (cf. Figure S1) as proposed in the literature.[82−84] We used the same values for both molecules: Δ = 6.5 eV, *U* = 6 eV, and *T* = 1 eV. *U* includes both the intraorbital interaction strength (U_{dd}) and the interorbital interaction strength (U_{dp}). We note that the influence of the LMCT is rather small (about 90% d^6 and 10% d^7 configurations). Even by omitting LMCT completely, all conclusions for the electronic configurations remain valid; only the determined crystal field parameters are slightly shifted. The XA and XMCD spectra were calculated for normal (90°) and grazing incidence (30°) by using appropriate beam vectors to adopt the experimental conditions. We would like to point out the complexity of reproducing four different spectra (XAS and XMCD for normal and grazing incidence, respectively) with just one set of parameters. This approach considerably increases the reliability of the obtained results compared to a calculation of a single XA spectrum.

The program CTM4XAS was used to perform a large number of calculations with an automated parameter variation for spectra at normal incidence. This is a crucial condition to gain an easy access to the two parameter plots. With Crispy,[66] spectra for grazing incidence were calculated. It was ensured that for the same parameters the same results are obtained with each program, considering the different definition of Slater integrals for the Coulomb interaction (CTM4XAS: atomic value, Crispy: Hartree−Fock value). The values given in this paper are scaled with respect to the Hartree−Fock value.

Because FePc and $FePcF_{16}$ exhibit specific magnetic properties, a combination of characteristic features can be used as markers to find parameter regions where the calculated spectra are like the experiment. For this purpose, the intensity of the XMCD, the L_3/L_2 branching ratio, and the spin and orbital magnetic momentum are used. In this manner, the experimental XMCD signal can be reproduced very well. The following parameter plots are shown for *Ds* values with best agreement to experimental data.

In the two parameter plots of FePc shown in Figure 3a,b *Dq* and *Dt* were varied for a fixed *Ds*, Coulomb interaction, and spin−orbit coupling. The values for the intensity of the XMCD in the first column are obtained by the integral over the absolute values of the XMCD signal. From this result it becomes obvious in which regions the spectra show a clear magnetism for normal and grazing incidence, respectively. In a

next step, these magnetic features can be investigated concerning their spin and orbital magnetic momentum. Just using a large number of automatically calculated spectra, we can rule out the vast majority of parameter combinations. A stripe like region in the upper right corner of the two parameter plots is the only one that fulfills all conditions since it shows a strong magnetism with a high positive orbital magnetic momentum and a negative spin magnetic momentum as it was determined from the experimental results.

With the profiles in Figure 3c we monitor changes of the magnetic properties in detail—in particular, the two transitions at *Dt* values of 0.21 and 0.27. Below *Dt* = 0.21 there is no magnetism due to a singlet state with an electron configuration $(b_{2g})^2(e_g)^4$. The first transition (*Dt* = 0.21) is marked by a strong increase in XMCD and m_l for normal incidence accompanied by a slowly decreasing m_s^{eff}. At grazing incidence, the XMCD is significantly less intense with a similar m_l but a positive m_s^{eff}. The region between *Dt* = 0.21 and 0.27 is characterized by a ^3E_g ground state with a $(b_{2g})^2(e_g)^3(a_{1g})^1$ configuration. The second transition (*Dt* = 0.27) shows an opposing trend under normal incidence with an abrupt decrease of XMCD, m_l, and m_s^{eff} to almost zero. For grazing incidence all parameters show a sharp positive peak with a maximum directly at the transition site. Above *Dt* = 0.27 the ground state changes to $^3A_{2g}$ with $(b_{2g})^2(e_g)^2(a_{1g})^2$.

Finally, we can determine the calculation parameters that describe the experimental data very well. The crystal field parameters for FePc are *Dq* = 0.29, *Ds* = 0.50, and *Dt* = 0.271, the reduction of the Slater integrals was 60%, and a small increase of the spin−orbit coupling from 1.00 to 1.01 was found. The lowering of the Slater integrals to 60% of the Hartree−Fock value is in a good agreement with literature, where for FePc values between 60% and 70% were reported.[46,47,49] In general, a small reduction is reasonable to compensate for the overestimation of electron−electron repulsion. A further decrease to 60% can be understood by a bonding between Fe and the neighboring atoms, which is not purely ionic but partly covalent.[85,86] With these parameters FePc is directly at the second transition (at higher *Dt* values), marked with horizontal dashes in Figure 3. This transition marks the change from a ^3E_g configuration with $(b_{2g})^2(e_g)^3(a_{1g})^1$ to a $^3A_{2g}$ ground state with $(b_{2g})^2(e_g)^2(a_{1g})^2$. At this point, the XMCD signal for normal incidence is still sufficient, but we take advantage of the strong increase for grazing incidence. One must keep in mind that locating the parameter set for the molecule directly at a transition of the electronic configuration implies that even small changes of the environment can cause a dramatic change of the magnetic properties and the electronic ground state. Thus, an increase of the *Dt* value by only 0.001 changes the contribution of ^3E_g and $^3A_{2g}$ configuration by up to 25%. This explains the large variation of results for the electron configuration of FePc in the literature. Applying the obtained *Ds* and *Dt* values to the parameter plots by Kuz'min et al.,[45] the electronic config uration of FePc is located in the region T_3 in the notation of ref 45, corresponding to a ^3E_g configuration. We note that it was suggested that the detailed molecular arrangement involving a hybridization between adjacent molecules may distinctly affect the ground state,[47] and the ^3E_g ground state might be a property of FePc in thin films or α FePc single crystals.[47,51] In agreement with our experimental results, a large magnetic orbital momentum for a ^3E_g configuration was found theoretically[47] and experimentally.[74] In addition, the double occupied b_{2g} with just one electron in a_{1g} is in good agreement with the recent results for FePc.[46]

For $FePcF_{16}$, the best parameters were determined to be *Dq* = 0.25, *Ds* = 0.45, and *Dt* = 0.220, Slater integrals reduced to 60%, and a spin−orbit coupling of 1.02 (Figure S3). Because *Ds*, reduction of the Slater integrals, and spin−orbit coupling vary only on a small scale for both molecules, the two parameter plot for $FePcF_{16}$ is similar to FePc. The parameter set in Figure S3b is located slightly lower in the region between the two transitions of the electronic configuration (see vertical lines with horizontal dashes), where the XMCD is strong for normal but rather weak for grazing incidence. Thus, we arrive at a position for $FePcF_{16}$ in the two parameter plot which is close to FePc but clearly indicates a ground state with ^3E_g configuration and $(b_{2g})^2(e_g)^3(a_{1g})^1$, in accordance with recent calculations.[87] This similarity agrees well with calculations of the relative energies of different electron configurations, where only a small difference between FePc and $FePcF_{16}$ was found, with ^3E_g and $^3A_{2g}$ close to each other.[88] Hence, the perfluorination influences the crystal field splitting and thus the energetic position of the d levels but does not change the ground state, most likely due to the electron withdrawing effect of the fluorine atoms. Upon comparison of the two parameter plots in Figure 3 and Figure S3, the transitions are farther away for $FePcF_{16}$ as for FePc. Consequently, magnetic properties of $FePcF_{16}$ are comparably more stable against small changes of the calculation parameters. Aside from the crystal field parameters *Dq* and *Dt*, there is no large difference in Coulomb interaction, spin−orbit coupling, and *Ds* for both calculations. Indeed, we have found a noticeably reduced crystal field interaction for $FePcF_{16}$.

Based on these parameters XA and XMCD spectra were calculated, presented in Figure 4 together with experimental

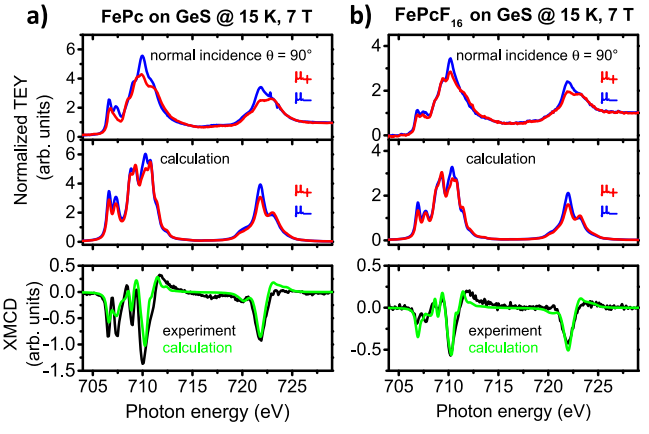

Figure 4. Simulated XA and XMCD spectra of (a) FePc and (b) $FePcF_{16}$ in comparison with the experimental spectra of (a) FePc and (b) $FePcF_{16}$ thin films on GeS at normal incidence.

data for normal incidence. The calculated spectra were broadened with a constant Gaussian function (experimental resolution) and a Lorentzian function incremented in width over the spectra from L_3 to L_2 (finite lifetime of core hole states). The agreement with the experimental spectra is significantly increased if a small tilt of the molecules against the substrate surface of ~20° is allowed. Note that this value is almost in agreement with the data obtained from the linearly polarized measurements of the N K edge absorption spectra above. The main features of the XA spectra are present in the

calculations, in particular the double peak in the L_3 edge around 707 eV. The overall shape resembles the experimental results for FePc as well as $FePcF_{16}$ except the strong dip at around 709 eV which could be related to an insufficient broadening of the states between 708 and 709 eV. The best agreement is obtained for the XMCD signals, which show four peaks at the L_3 edge and one at the L_2, all of them pointing downward. The calculation for a flat lying molecule can explain all features except the second XMCD peak in the L_3 edge at 707.5 eV. This peak originates most likely from a tilting of the molecules because it is the most intense XMCD peak for grazing incidence (cf. Figure 5).

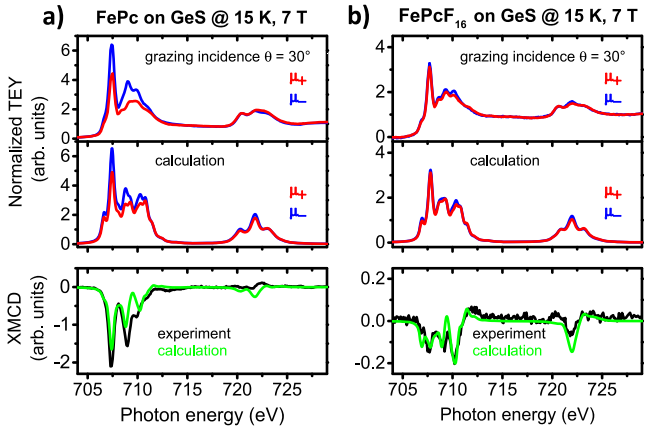

Figure 5. Simulated XA and XMCD spectra of (a) FePc and (b) $FePcF_{16}$ in comparison with the experimental spectra of (a) FePc and (b) $FePcF_{16}$ thin films on GeS at grazing incidence.

While the obtained results for FePc and $FePcF_{16}$ are very similar at normal incidence, there are significant differences for grazing incidence, shown in Figure 5. FePc exhibits a large XMCD signal at the L_3 edge but almost none at the L_2 edge. On the contrary, $FePcF_{16}$ has a very weak XMCD including a small dip at the L_2 edge. As for normal incidence a tilting of the molecules was also considered for the grazing incidence calculations. Contributions from different tilt directions of the molecules at the same tilt angle were appropriately averaged to take several azimuthal orientations into account with respect to the incoming radiation. Here, the influence of the molecular tilting can be seen by the XMCD peak at 710.5 eV, which is the most intense one for normal incidence. In both cases the strong dip at around 709 eV is still present, but the shape of the XAS as well as the XMCD is reflected in the calculations. Now the question arises if the difference in the electronic structure of the central iron ion in FePc and $FePcF_{16}$ is a direct consequence of the chemical modification; that is, the fluorination changes the extent of hybridization between phthalocyanine π orbitals and Fe states. The slight differences in the shape of N K edge absorption spectra for FePc and $FePcF_{16}$ (cf. Figure 1) might indicate a different electronic structure. On the other hand, strong differences in the crystal field parameters for single FePc and $FePcF_{16}$ molecules are not expected.[67] However, for related phthalocyanines a significant impact of the fluorination on the single crystal structure and arrangement in thin films was observed.[53−56] This may affect intermolecular interactions including local interactions between iron atoms of a Pc molecule and atoms of neighboring Pc molecules (Fe or N).

Our multiplet calculations show that even small changes in the parameter set can have large impact on the XMCD effect, which makes it obvious that the molecular arrangement needs to be considered. From the N K edge adsorption spectrum, we expect mostly flat lying molecules; the estimated tilt angle was up to 25° for both molecules. Additionally, the agreement of calculated XMCD spectra with experimental data was improved by introducing such tilt angles into the calculations. Thus, it might be reasonable to assume that the FePc and $FePcF_{16}$ thin films have a structure similar to α FePc, where the molecules are stacked parallel to each other along the short axis at intervals of 3.78 Å (which also correspond to the Fe−Fe distance), and the molecular planes are inclined to the crystallographic *ac* plane by an angle of 26.5°.[44] In the α form, the nearest neighbors from adjacent molecules to the Fe atom are nitrogen atoms. It is very reasonable to assume that the Fe−Fe separation distance and the angle of inclination substantially affect the extent of collective magnetic interactions.[44] The XMCD measurements of this study were conducted in an intermediate temperature regime (5−25 K), where α FePc is expected to be still paramagnetic, but short range interactions within a Pc column are already possible.[43] The fluorination of FePc might change details in the intermolecular arrangement, as the Fe−Fe distance or the angle of inclination, which might render the coupling of neighboring Fe atoms less effective.

We note that the appearance of collective magnetic phenomena such as a ferromagnetic or antiferromagnetic coupling was reported for related phthalocyanines. For single crystalline β MnPc, an exchange coupling via the π orbitals of the phthalocyanine ring was suggested, resulting in a ferromagnetic coupling at low temperatures (8.6 K).[31] In this case, the nitrogen atoms of the phthalocyanine as nearest neighbors to the central metal atom are involved in the interaction. Assuming similar interactions for the investigated iron phthalocyanines, an XMCD signal might be expected at the N K edge. Indeed, in Figure 6 we see a weak negative

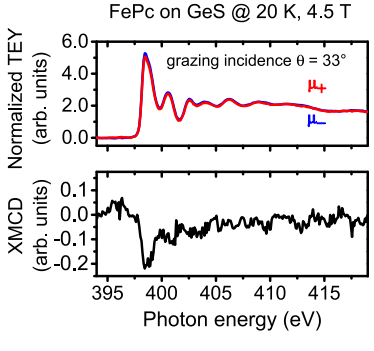

Figure 6. XMCD spectra at the N K edge of an about 3 nm thick FePc film at low temperature. A weak XMCD signal is clearly visible. The **k** vector of the circularly polarized light either parallel (μ_+, red spectrum) or antiparallel (μ_-, blue spectrum).

XMCD signal for FePc in thin films at low temperature. This signal shows that the Fe atoms induce a magnetic moment in the surrounding nitrogen atoms parallel to the magnetic moment of the iron atom. The appearance of such a polarized band points to a crucial role of the nitrogen atoms in the interaction between different FePc molecules and/or the interaction between the central Fe atom and the macrocycle.

The XMCD signal at the N K edge will be investigated more extensively in further studies.

4. SUMMARY

We studied the electronic structure of the central iron ion of iron phthalocyanine and perfluorinated iron phthalocyanine thin films on a weakly interacting substrate by the means of XAS, XMCD, and multiplet calculations. Both 3 nm thick FePc and $FePcF_{16}$ films are highly ordered with the molecule lying mostly flat on the surface, facilitating the analysis of the (unoccupied) electronic structure of the central Fe ion. The polarization dependent XA spectra of Fe $L_{2,3}$ edges obtained by using linearly polarized light exhibit distinct differences for FePc and $FePcF_{16}$. FePc and $FePcF_{16}$ films show an XMCD signal at 15 K and 7 T, but both the intensity and shape of the XMCD are different. The XMCD effect for FePc is larger compared to $FePcF_{16}$, especially at grazing incidence. This leads to a much larger orbital moment for FePc parallel to the substrate plane and a larger spin moment. The drastic changes of the XMCD can be well reproduced by multiplet calculations. The calculations show that extremely small changes in the ligand field parameters have large impact on the XMCD signal and thus on magnetic moments. Therefore, we propose that differences in the electronic structure arise from subtle differences in the molecular arrangement of FePc and $FePcF_{16}$ molecules in thin films. To shed more light on the interplay between molecular arrangement and electronic structure of the central Fe ion, XMCD studies on partial fluorinated iron phthalocyanine in thin films is planned. In addition, the size of the XMCD signal will be investigated for differently fluorinated Fe phthalocyanines.

■ ASSOCIATED CONTENT

● Supporting Information

The Supporting Information is available free of charge at https://pubs.acs.org/doi/10.1021/acs.jpcc.0c11591.

> Fe $2p_{3/2}$ core level spectra of FePc and $FePcF_{16}$ thin films on GeS; XMCD signals of FePc and $FePcF_{16}$ in dependence of magnetic field strength; calculation of the magnetic moments according to the sum rules; two parameter plots of $FePcF_{16}$ for normal and grazing incidence with the calculation parameters *Dq* and *Dt* (PDF)

■ AUTHOR INFORMATION

Corresponding Author

Heiko Peisert − *Institute of Physical and Theoretical Chemistry, University of Tübingen, 72076 Tübingen, Germany*; orcid.org/0000 0002 9742 5800; Phone: (+49) 07071; Email: heiko.peisert@uni tuebingen.de; Fax: (+49) 07071

Authors

Katharina Greulich − *Institute of Physical and Theoretical Chemistry, University of Tübingen, 72076 Tübingen, Germany*

Martin Trautmann − *Institute of Physics, Martin Luther University Halle−Wittenberg, 06120 Halle, Germany*

Axel Belser − *Institute of Physical and Theoretical Chemistry, University of Tübingen, 72076 Tübingen, Germany*

Sven Bölke − *Institute of Physical and Theoretical Chemistry, University of Tübingen, 72076 Tübingen, Germany*

Reimer Karstens − *Institute of Physical and Theoretical Chemistry, University of Tübingen, 72076 Tübingen, Germany*

Peter Nagel − *Institute for Quantum Materials and Technologies (IQMT), Karlsruhe Institute of Technology (KIT), 76021 Karlsruhe, Germany*

Stefan Schuppler − *Institute for Quantum Materials and Technologies (IQMT), Karlsruhe Institute of Technology (KIT), 76021 Karlsruhe, Germany*

Michael Merz − *Institute for Quantum Materials and Technologies (IQMT), Karlsruhe Institute of Technology (KIT), 76021 Karlsruhe, Germany*

Angelika Chassé − *Institute of Physics, Martin Luther University Halle−Wittenberg, 06120 Halle, Germany*

Thomas Chassé − *Institute of Physical and Theoretical Chemistry, University of Tübingen, 72076 Tübingen, Germany; Center for Light−Matter Interaction, Sensors & Analytics (LISA$^+$), University of Tübingen, 72076 Tübingen, Germany*; orcid.org/0000 0001 6442 8944

Complete contact information is available at: https://pubs.acs.org/10.1021/acs.jpcc.0c11591

Notes

The authors declare no competing financial interest.

■ ACKNOWLEDGMENTS

Financial support from the DFG through the framework of the SFB 762, "Functionality of Oxide Interfaces", is gratefully acknowledged. The authors acknowledge support by the state of Baden Württemberg through bwHPC and the German Research Foundation (DFG) through Grant INST 40/467 1 FUGG (JUSTUS cluster). We thank H. Adler (University of Tübingen) for valuable discussions and technical support. We are grateful to the synchrotron light source KARA and to KNMF, both Karlsruhe, Germany, for the provision of beamtime.

■ REFERENCES

(1) Kuch, W. G.; Bernien, M. Controlling the Magnetism of Adsorbed Metal Organic Molecules. *J. Phys. Condes. Matter* **2017**, *29*, 14.

(2) Gottfried, J. M. Surface Chemistry of Porphyrins and Phthalocyanines. *Surf. Sci. Rep.* **2015**, *70*, 259−379.

(3) Walzer, K.; Maennig, B.; Pfeiffer, M.; Leo, K. Highly Efficient Organic Devices Based on Electrically Doped Transport Layers. *Chem. Rev.* **2007**, *107*, 1233−1271.

(4) Martinez Diaz, M. V.; de la Torre, G.; Torres, T. Lighting Porphyrins and Phthalocyanines for Molecular Photovoltaics. *Chem. Commun.* **2010**, *46*, 7090−7108.

(5) Sanvito, S. Molecular Spintronics. *Chem. Soc. Rev.* **2011**, *40*, 3336−3355.

(6) Chen, H.; Zhang, W.; Li, M.; He, G.; Guo, X. Interface Engineering in Organic Field Effect Transistors: Principles, Applica tions, and Perspectives. *Chem. Rev.* **2020**, *120*, 2879−2949.

(7) Zhao, H.; He, Z.; Zhang, X.; Zhang, Z.; Diyaf, A.; Lind, A. H. N.; Liang, C.; Wilson, J. I. B. A Preliminary Investigation into Hybrid Photovoltaic Cells with Organic Phthalocyanines and Amorphous Silicon Heterojunction. *J. Phys. D: Appl. Phys.* **2015**, *48*, 195102.

(8) Sun, Y.; Li, X.; Wang, S.; Zhang, L.; Ma, F. Synthesis, Spectral Properties of Zinc Hexadecafluorophthalocyanine ($Znpcf_{16}$) and Its Application in Organic Thin Film Transistors. *Mater. Trans.* **2017**, *58*, 103−106.

(9) Bilgiçli, A. T.; Yaraşır, M. N.; Kandaz, M.; İlik, C.; Demir, A.; Bağcı, S. Nonperipheral Tetra Phthalocyanines Bearing Alkyl Chain

Moiety; Synthesis, Characterization and Fabrication of the Ofet Based on Phthalocyanine. *Synth. Met.* **2015**, *206*, 33−41.
(10) Warner, M.; Din, S.; Tupitsyn, I. S.; Morley, G. W.; Stoneham, A. M.; Gardener, J. A.; Wu, Z.; Fisher, A. J.; Heutz, S.; Kay, C. W. M.; Aeppli, G.; et al. Potential for Spin Based Information Processing in a Thin Film Molecular Semiconductor. *Nature* **2013**, *503*, 504−508.
(11) Domingo, N.; Bellido, E.; Ruiz Molina, D. Advances on Structuring, Integration and Magnetic Characterization of Molecular Nanomagnets on Surfaces and Devices. *Chem. Soc. Rev.* **2012**, *41*, 258−302.
(12) Annese, E.; Fujii, J.; Vobornik, I.; Panaccione, G.; Rossi, G. Control of the Magnetism of Cobalt Phthalocyanine by a Ferromagnetic Substrate. *Phys. Rev. B* **2011**, *84*, 174443.
(13) Cinchetti, M.; Heimer, K.; Wustenberg, J. P.; Andreyev, O.; Bauer, M.; Lach, S.; Ziegler, C.; Gao, Y. L.; Aeschlimann, M. Determination of Spin Injection and Transport in a Ferromagnet/Organic Semiconductor Heterojunction by Two Photon Photo emission. *Nat. Mater.* **2009**, *8*, 115−119.
(14) Liu, Y.; Lee, T.; Katz, H. E.; Reich, D. H. Effects of Carrier Mobility and Morphology in Organic Semiconductor Spin Valves. *J. Appl. Phys.* **2009**, *105*, No. 07c708.
(15) Schmitt, F.; Sauther, J.; Lach, S.; Ziegler, C. Characterization of the Interface Interaction of Cobalt on Top of Copper and Iron Phthalocyanine. *Anal. Bioanal. Chem.* **2011**, *400*, 665−671.
(16) Petraki, F.; Peisert, H.; Aygul, U.; Latteyer, F.; Uihlein, J.; Vollmer, A.; Chassé, T. Electronic Structure of FePc and Interface Properties on Ag(111) and Au(100). *J. Phys. Chem. C* **2012**, *116*, 11110−11116.
(17) Betti, M. G.; Gargiani, P.; Frisenda, R.; Biagi, R.; Cossaro, A.; Verdini, A.; Floreano, L.; Mariani, C. Localized and Dispersive Electronic States at Ordered FePc and CoPc Chains on Au(110). *J. Phys. Chem. C* **2010**, *114*, 21638−21644.
(18) Gargiani, P.; Rossi, G.; Biagi, R.; Corradini, V.; Pedio, M.; Fortuna, S.; Calzolari, A.; Fabris, S.; Cezar, J. C.; Brookes, N. B.; et al. Spin and Orbital Configuration of Metal Phthalocyanine Chains Assembled on the Au(110) Surface. *Phys. Rev. B: Condens. Matter Mater. Phys.* **2013**, *87*, 165407.
(19) Peisert, H.; Uihlein, J.; Petraki, F.; Chassé, T. Charge Transfer between Transition Metal Phthalocyanines and Metal Substrates: The Role of the Transition Metal. *J. Electron Spectrosc. Relat. Phenom.* **2015**, *204*, 49−60.
(20) Klar, D.; Brena, B.; Herper, H. C.; Bhandary, S.; Weis, C.; Krumme, B.; Schmitz Antoniak, C.; Sanyal, B.; Eriksson, O.; Wende, H. Oxygen Tuned Magnetic Coupling of Fe Phthalocyanine Mole cules to Ferromagnetic Co Films. *Phys. Rev. B: Condens. Matter Mater. Phys.* **2013**, *88*, 224424.
(21) Schmid, M.; Zirzlmeier, J.; Steinruck, H. P.; Gottfried, J. M. Interfacial Interactions of Iron(II) Tetrapyrrole Complexes on Au(111). *J. Phys. Chem. C* **2011**, *115*, 17028−17035.
(22) Stepanow, S.; Miedema, P. S.; Mugarza, A.; Ceballos, G.; Moras, P.; Cezar, J. C.; Carbone, C.; de Groot, F. M. F.; Gambardella, P. Mixed Valence Behavior and Strong Correlation Effects of Metal Phthalocyanines Adsorbed on Metals. *Phys. Rev. B: Condens. Matter Mater. Phys.* **2011**, *83*, 220401.
(23) Stepanow, S.; Lodi Rizzini, A.; Krull, C.; Kavich, J.; Cezar, J. C.; Yakhou Harris, F.; Sheverdyaeva, P. M.; Moras, P.; Carbone, C.; Ceballos, G.; et al. Spin Tuning of Electron Doped Metal−Phthalocyanine Layers. *J. Am. Chem. Soc.* **2014**, *136*, 5451−5459.
(24) Johnson, P. S.; Garcia Lastra, J. M.; Kennedy, C. K.; Jersett, N. J.; Boukahil, I.; Himpsel, F. J.; Cook, P. L. Crystal Fields of Porphyrins and Phthalocyanines from Polarization Dependent 2p to 3d Multip lets. *J. Chem. Phys.* **2014**, *140*, 8.
(25) Avvisati, G.; Lisi, S.; Gargiani, P.; Della Pia, A.; De Luca, O.; Pacile, D.; Cardoso, C.; Varsano, D.; Prezzi, D.; Ferretti, A.; et al. FePc Adsorption on the Moire Superstructure of Graphene Intercalated with a Cobalt Layer. *J. Phys. Chem. C* **2017**, *121*, 1639−1647.
(26) Avvisati, G.; Cardoso, C.; Varsano, D.; Ferretti, A.; Gargiani, P.; Betti, M. G. Ferromagnetic and Antiferromagnetic Coupling of Spin Molecular Interfaces with High Thermal Stability. *Nano Lett.* **2018**, *18*, 2268−2273.
(27) Uihlein, J.; Polek, M.; Glaser, M.; Adler, H.; Ovsyannikov, R.; Bauer, M.; Ivanovic, M.; Preobrajenski, A. B.; Generalov, A. V.; Chassé, T.; et al. Influence of Graphene on Charge Transfer between CoPc and Metals: The Role of Graphene−Substrate Coupling. *J. Phys. Chem. C* **2015**, *119*, 15240−15247.
(28) Lodi Rizzini, A.; Krull, C.; Mugarza, A.; Balashov, T.; Nistor, C.; Piquerel, R.; Klyatskaya, S.; Ruben, M.; Sheverdyaeva, P. M.; Moras, P.; et al. Coupling of Single, Double, and Triple Decker Metal Phthalocyanine Complexes to Ferromagnetic and Antiferromagnetic Substrates. *Surf. Sci.* **2014**, *630*, 361−374.
(29) Hermanns, C. F.; Tarafder, K.; Bernien, M.; Kruger, A.; Chang, Y. M.; Oppeneer, P. M.; Kuch, W. Magnetic Coupling of Porphyrin Molecules through Graphene. *Adv. Mater.* **2013**, *25*, 3473−3477.
(30) Bernien, M.; Miguel, J.; Weis, C.; Ali, M. E.; Kurde, J.; Krumme, B.; Panchmatia, P. M.; Sanyal, B.; Piantek, M.; Srivastava, P.; et al. Tailoring the Nature of Magnetic Coupling of Fe Porphyrin Molecules to Ferromagnetic Substrates. *Phys. Rev. Lett.* **2009**, *102*, 4.
(31) Kataoka, T.; Sakamoto, Y.; Yamazaki, Y.; Singh, V. R.; Fujimori, A.; Takeda, Y.; Ohkochi, T.; Fujimori, S. I.; Okane, T.; Saitoh, Y.; et al. Electronic Configuration of Mn Ions in the pi D Molecular Ferromagnet Beta Mn Phthalocyanine Studied by Soft X Ray Magnetic Circular Dichroism. *Solid State Commun.* **2012**, *152*, 806−809.
(32) Cojocariu, I.; Carlotto, S.; Sturmeit, H. M.; Zamborlini, G.; Cinchetti, M.; Cossaro, A.; Verdini, A.; Floreano, L.; Jugovac, M.; Puschnig, P. Ferrous to Ferric Transition in Fe Phthalocyanine Driven by NO_2 Exposure. *Chem.—Eur. J.* **2021**, DOI: 10.1002/chem.202004932.
(33) Stepanow, S.; Mugarza, A.; Ceballos, G.; Moras, P.; Cezar, J. C.; Carbone, C.; Gambardella, P. Giant Spin and Orbital Moment Anisotropies of a Cu Phthalocyanine Monolayer. *Phys. Rev. B: Condens. Matter* **2010**, *82*, 014405.
(34) Halcrow, M. A. The Effect of Ligand Design on Metal Ion Spin State Lessons from Spin Crossover Complexes. *Crystals* **2016**, *6*, 58.
(35) Miedema, P. S.; de Groot, F. M. F. The Iron L Edges: Fe 2p X Ray Absorption and Electron Energy Loss Spectroscopy. *J. Electron Spectrosc. Relat. Phenom.* **2013**, *187*, 32−48.
(36) Miedema, P. S.; Stepanow, S.; Gambardella, P.; de Groot, F. M. F. 2p X Ray Absorption of Iron Phthalocyanine. In *14th International Conference on X Ray Absorption Fine Structure*; DiCicco, A., Filipponi, A., Eds.; Iop Publishing Ltd.: Bristol, 2009; Vol. *190*.
(37) Kuz'min, M. D.; Hayn, R.; Oison, V. Ab Initio Calculated XANES and XMCD Spectra of Fe(II) Phthalocyanine. *Phys. Rev. B: Condens. Matter Mater. Phys.* **2009**, *79*, No. 024413.
(38) Bernien, M.; Xu, X.; Miguel, J.; Piantek, M.; Eckhold, P.; Luo, J.; Kurde, J.; Kuch, W.; Baberschke, K.; Wende, H. Fe Porphyrin Monolayers on Ferromagnetic Substrates: Electronic Structure and Magnetic Coupling Strength. *Phys. Rev. B* **2007**, *76*, 214406.
(39) Kuepper, K.; Benoit, D. M.; Wiedwald, U.; Moegele, F.; Meyering, A.; Neumann, M.; Kappler, J. P.; Joly, L.; Weidle, S.; Rieger, B.; et al. Precise Chemical, Electronic, and Magnetic Structure of Binuclear Complexes Studied by Means of X Ray Spectroscopies and Theoretical Methods. *J. Phys. Chem. C* **2011**, *115*, 25030−25039.
(40) Nakajima, R.; Stohr, J.; Idzerda, Y. U. Electron Yield Saturation Effects in L Edge X Ray Magnetic Circular Dichroism Spectra of Fe, Co, and Ni. *Phys. Rev. B: Condens. Matter Mater. Phys.* **1999**, *59*, 6421−6429.
(41) Scheybal, A.; Ramsvik, T.; Bertschinger, R.; Putero, M.; Nolting, F.; Jung, T. A. Induced Magnetic Ordering in a Molecular Monolayer. *Chem. Phys. Lett.* **2005**, *411*, 214−220.
(42) Girovsky, J.; Nowakowski, J.; Ali, E.; Baljozovic, M.; Rossmann, H. R.; Nijs, T.; Aeby, E. A.; Nowakowska, S.; Siewert, D.; Srivastava, G.; et al. Long Range Ferrimagnetic Order in a Two Dimensional Supramolecular Kondo Lattice. *Nat. Commun.* **2017**, *8*, 8.
(43) Gredig, T.; Colesniuc, C. N.; Crooker, S. A.; Schuller, I. K. Substrate Controlled Ferromagnetism in Iron Phthalocyanine Films

Due to One Dimensional Iron Chains. *Phys. Rev. B: Condens. Matter Mater. Phys.* **2012**, *86*, No. 014409.
(44) Evangelisti, M.; Bartolomé, J.; de Jongh, L. J.; Filoti, G. Magnetic Properties of α Iron(II) Phthalocyanine. *Phys. Rev. B: Condens. Matter Mater. Phys.* **2002**, *66*, 144410.
(45) Kuz'min, M. D.; Savoyant, A.; Hayn, R. Ligand Field Parameters and the Ground State of Fe(II) Phthalocyanine. *J. Chem. Phys.* **2013**, *138*, 244308.
(46) Natoli, C. R.; Kruger, P.; Bartolome, J.; Bartolome, F. Determination of the Ground State of an Au Supported FePc Film Based on the Interpretation of Fe K and L Edge X Ray Magnetic Circular Dichroism Measurements. *Phys. Rev. B* **2018**, *97*, 16.
(47) Nakamura, K.; Kitaoka, Y.; Akiyama, T.; Ito, T.; Weinert, M.; Freeman, A. J. Constraint Density Functional Calculations for Multiplets in a Ligand Field Applied to Fe Phthalocyanine. *Phys. Rev. B: Condens. Matter Mater. Phys.* **2012**, *85*, 235129.
(48) Kitaoka, Y.; Nakamura, K.; Akiyama, T.; Ito, T.; Weinert, M.; Freeman, A. J. Magnetism and Multiplets in Fe Phthalocyanine Molecules. *J. Korean Phys. Soc.* **2013**, *63*, 695−698.
(49) Dale, B. W.; Williams, R. J. P.; Johnson, C. E.; Thorp, T. L. S = 1 Spin State of Divalent Iron. I. Magnetic Properties of Phthalocyanine Iron (II). *J. Chem. Phys.* **1968**, *49*, 3441−3444.
(50) Fernández Rodríguez, J.; Toby, B.; van Veenendaal, M. Mixed Configuration Ground State in Iron(II) Phthalocyanine. *Phys. Rev. B: Condens. Matter Mater. Phys.* **2015**, *91*, 214427.
(51) Bidermane, I.; Brumboiu, I. E.; Totani, R.; Grazioli, C.; Shariati Nilsson, M. N.; Herper, H. C.; Eriksson, O.; Sanyal, B.; Ressel, B.; de Simone, M.; et al. Atomic Contributions to the Valence Band Photoelectron Spectra of Metal Free, Iron and Manganese Phthalocyanines. *J. Electron Spectrosc. Relat. Phenom.* **2015**, *205*, 92−97.
(52) Bartolomé, J.; Bartolomé, F.; Figueroa, A. I.; Bunău, O.; Schuller, I. K.; Gredig, T.; Wilhelm, F.; Rogalev, A.; Krüger, P.; Natoli, C. R. Quadrupolar XMCD at the Fe K Edge in Fe Phthalocyanine Film on Au: Insight into the Magnetic Ground State. *Phys. Rev. B: Condens. Matter Mater. Phys.* **2015**, *91*, 220401.
(53) Basova, T. V.; Kiselev, V. G.; Dubkov, I. S.; Latteyer, F.; Gromilov, S. A.; Peisert, H.; Chasse, T. Optical Spectroscopy and Xrd Study of Molecular Orientation, Polymorphism, and Phase Tran sitions in Fluorinated Vanadyl Phthalocyanine Thin Films. *J. Phys. Chem. C* **2013**, *117*, 7097−7106.
(54) Schuster, B. E.; Basova, T. V.; Plyashkevich, V. A.; Peisert, H.; Chasse, T. Effects of Temperature on Structural and Morphological Features of CoPc and CoPcF16 Thin Films. *Thin Solid Films* **2010**, *518*, 7161−7166.
(55) Klyamer, D. D.; Sukhikh, A. S.; Krasnov, P. O.; Gromilov, S. A.; Morozova, N. B.; Basova, T. V. Thin Films of Tetrafluorosubstituted Cobalt Phthalocyanine: Structure and Sensor Properties. *Appl. Surf. Sci.* **2016**, *372*, 79−86.
(56) Sukhikh, A. S.; Klyamer, D. D.; Parkhomenko, R. G.; Krasnov, P. O.; Gromilov, S. A.; Hassan, A. K.; Basova, T. V. Effect of Fluorosubstitution on the Structure of Single Crystals, Thin Films and Spectral Properties of Palladium Phthalocyanines. *Dyes Pigm.* **2018**, *149*, 348−355.
(57) Belser, A.; Karstens, R.; Nagel, P.; Merz, M.; Schuppler, S.; Chassé, T.; Peisert, H. Interaction Channels between Perfluorinated Iron Phthalocyanine and Cu(111). *Phys. Status Solidi B* **2019**, *256*, 1800292.
(58) Thole, B. T.; Carra, P.; Sette, F.; Vanderlaan, G. X Ray Circular Dichroism as a Probe of Orbital Magnetization. *Phys. Rev. Lett.* **1992**, *68*, 1943−1946.
(59) Carra, P.; Thole, B. T.; Altarelli, M.; Wang, X. D. X Ray Circular Dichroism and Local Magnetic Fields. *Phys. Rev. Lett.* **1993**, *70*, 694−697.
(60) Stöhr, J. Exploring the Microscopic Origin of Magnetic Anisotropies with X Ray Magnetic Circular Dichroism (XMCD) Spectroscopy. *J. Magn. Magn. Mater.* **1999**, *200*, 470−497.
(61) Weser, M.; Rehder, Y.; Horn, K.; Sicot, M.; Fonin, M.; Preobrajenski, A. B.; Voloshina, E. N.; Goering, E.; Dedkov, Y. S. Induced Magnetism of Carbon Atoms at the Graphene/Ni(111) Interface. *Appl. Phys. Lett.* **2010**, *96*, 012504.
(62) Yeh, J. J.; Lindau, I. Atomic Subshell Photoionization Cross Sections and Asymmetry Parameters: $1 \leqslant Z \leqslant 103$. *At. Data Nucl. Data Tables* **1985**, *32*, 1−155.
(63) Seah, M. P.; Dench, W. A. Quantitative Electron Spectroscopy of Surfaces: A Standard Data Base for Electron Inelastic Mean Free Paths in Solids. *Surf. Interface Anal.* **1979**, *1*, 2−11.
(64) Stavitski, E.; de Groot, F. M. F. The Ctm4xas Program for EELS and XAS Spectral Shape Analysis of Transition Metal L Edges. *Micron* **2010**, *41*, 687−694.
(65) Delgado Jaime, M. U.; Zhang, K. L.; Vura Weis, J.; de Groot, F. M. F. Ctm4doc: Electronic Structure Analysis from X Ray Spectros copy. *J. Synchrotron Radiat.* **2016**, *23*, 1264−1271.
(66) *Crispy: V0.7.3*, 2019.
(67) Belser, A.; Karstens, R.; Grüninger, P.; Nagel, P.; Merz, M.; Schuppler, S.; Suturina, E. A.; Chassé, A.; Chassé, T.; Peisert, H. Spin State in Perfluorinated FePc Films on Cu(111) and Ag(111) in Dependence on Film Thickness. *J. Phys. Chem. C* **2018**, *122*, 15390−15394.
(68) Stöhr, J. *NEXAFS Spectroscopy;* Springer: 1992.
(69) Stöhr, J.; Outka, D. A. Determination of Molecular Orientations on Surfaces from the Angular Dependence of Near Edge X Ray Absorption Fine Structure Spectra. *Phys. Rev. B: Condens. Matter Mater. Phys.* **1987**, *36*, 7891−7905.
(70) Peisert, H.; Biswas, I.; Knupfer, M.; Chasse, T. Orientation and Electronic Properties of Phthalocyanines on Polycrystalline Sub strates. *Phys. Status Solidi B* **2009**, *246*, 1529−1545.
(71) Rocco, M. L. M.; Frank, K. H.; Yannoulis, P.; Koch, E. E. Unoccupied Electronic Structure of Phthalocyanine Films. *J. Chem. Phys.* **1990**, *93*, 6859−6864.
(72) de Groot, F. Multiplet Effects in X Ray Spectroscopy. *Coord. Chem. Rev.* **2005**, *249*, 31−63.
(73) Greulich, K.; Belser, A.; Bölke, S.; Grüninger, P.; Karstens, R.; Sättele, M. S.; Ovsyannikov, R.; Giangrisostomi, E.; Basova, T. V.; Klyamer, D.; et al. Charge Transfer from Organic Molecules to Molybdenum Disulfide: Influence of the Fluorination of Iron Phthalocyanine. *J. Phys. Chem. C* **2020**, *124*, 16990−16999.
(74) Bartolome, J.; Bartolome, F.; Garcia, L. M.; Filoti, G.; Gredig, T.; Colesniuc, C. N.; Schuller, I. K.; Cezar, J. C. Highly Unquenched Orbital Moment in Textured Fe Phthalocyanine Thin Films. *Phys. Rev. B* **2010**, *81*, 195405.
(75) Lisi, S.; Gargiani, P.; Scardamaglia, M.; Brookes, N. B.; Sessi, V.; Mariani, C.; Betti, M. G. Graphene Induced Magnetic Anisotropy of a Two Dimensional Iron Phthalocyanine Network. *J. Phys. Chem. Lett.* **2015**, *6*, 1690−1695.
(76) Altarelli, M. Orbital Magnetization Sum Rule for X Ray Circular Dichroism: A Simple Proof. *Phys. Rev. B: Condens. Matter Mater. Phys.* **1993**, *47*, 597−598.
(77) Stöhr, J.; König, H. Determination of Spin and Orbital Moment Anisotropies in Transition Metals by Angle Dependent X Ray Magnetic Circular Dichroism. *Phys. Rev. Lett.* **1995**, *75*, 3748−3751.
(78) Weller, D.; Stöhr, J.; Nakajima, R.; Carl, A.; Samant, M. G.; Chappert, C.; Mégy, R.; Beauvillain, P.; Veillet, P.; Held, G. A. Microscopic Origin of Magnetic Anisotropy in Au/Co/Au Probed with X Ray Magnetic Circular Dichroism. *Phys. Rev. Lett.* **1995**, *75*, 3752−3755.
(79) Chen, C. T.; Idzerda, Y. U.; Lin, H. J.; Smith, N. V.; Meigs, G.; Chaban, E.; Ho, G. H.; Pellegrin, E.; Sette, F. Experimental Confirmation of the X Ray Magnetic Circular Dichroism Sum Rules for Iron and Cobalt. *Phys. Rev. Lett.* **1995**, *75*, 152−155.
(80) Mabrouk, M.; Savoyant, A.; Giovanelli, L.; Clair, S.; Hayn, R.; Ben Chaabane, R. Ligand Influence on Local Magnetic Moments in Fe Based Metal−Organic Networks. *J. Phys. Chem. C* **2017**, *121*, 4253−4260.
(81) De Groot, F.; Kotani, A. *Core Level Spectroscopy of Solids*; CRC Press: 2008.

(82) Bocquet, A. E.; Fujimori, A. Predictions for Core Level X Ray Photoemission Spectra of Divalent and Trivalent 3d Transition Metal Compounds. *J. Electron Spectrosc. Relat. Phenom.* **1996**, *82*, 87−124.
(83) Fujimori, A.; Bocquet, A. E.; Saitoh, T.; Mizokawa, T. Electronic Structure of 3d Transition Metal Compounds: Systematic Chemical Trends and Multiplet Effects. *J. Electron Spectrosc. Relat. Phenom.* **1993**, *62*, 141−152.
(84) Bidermane, I.; Lüder, J.; Totani, R.; Grazioli, C.; de Simone, M.; Coreno, M.; Kivimäki, A.; Åhlund, J.; Lozzi, L.; Brena, B.; et al. Characterization of Gas Phase Iron Phthalocyanine with X Ray Photoelectron and Absorption Spectroscopies. *Phys. Status Solidi B* **2015**, *252*, 1259−1265.
(85) Zhou, J.; Zhang, L.; Hu, Z.; Kuo, C.; Liu, H.; Lin, X.; Wang, Y.; Pi, T. W.; Wang, J.; Zhang, S. The Significant Role of Covalency in Determining the Ground State of Cobalt Phthalocyanines Molecule. *AIP Adv.* **2016**, *6*, No. 035306.
(86) Liao, M. S.; Scheiner, S. Electronic Structure and Bonding in Metal Phthalocyanines, Metal = Fe, Co, Ni, Cu, Zn, Mg. *J. Chem. Phys.* **2001**, *114*, 9780−9791.
(87) Shati, K.; Javaid, S.; Khan, R. T. A.; Akhtar, M. J. Electronic Structure and Spin State of Fluorinated Metal Phthalocyanine Molecules. *J. Magn. Magn. Mater.* **2020**, *494*, 165775.
(88) Liao, M. S.; Watts, J. D.; Huang, M. J.; Gorun, S. M.; Kar, T.; Scheiner, S. Effects of Peripheral Substituents on the Electronic Structure and Properties of Unligated and Ligated Metal Phthalocya nines, Metal = Fe, Co, Zn. *J. Chem. Theory Comput.* **2005**, *1*, 1201−1210.